Numerical Aspects and Implementation of Population Balance Equations Coupled with Turbulent Fluid Dynamics

E. Bayraktar*, O. Mierka, F. Platte, D. Kuzmin and S. Turek

Institute of Applied Mathematics (LS III), University of Dortmund
Vogelpothsweg 87, D-44227, Dortmund, Germany.

E-mail: ebayrakt@math.uni-dortmund.de

Abstract

In this paper, we present numerical techniques for one-way coupling of CFD and Population Balance Equations (PBE) based on the incompressible flow solver FeatFlow which is extended with Chien's Low-Reynolds number $k-\varepsilon$ turbulence model, and breakage and coalescence closures. The presented implementation ensures strictly conservative treatment of sink and source terms which is enforced even for geometric discretization of the internal coordinate. The validation of our implementation which covers wide range of computational and experimental problems enables us to proceed into three-dimensional applications as, turbulent flows in a pipe and through a static mixer. The aim of this paper is to highlight the influence of different formulations of the novel theoretical breakage and coalescence models on the equilibrium distribution of population, and to propose an implementation strategy for three-dimensional one-way coupled CFD-PBE model.

1. Introduction

Population balances may be regarded either as an old subject that has its origin in the Boltzmann equation more than a century ago, or as a relatively new one in light of the variety of applications in which engineers have recently put population balances to use. Population balance equations (PBE) are essential to researchers of many distinct areas. Applications cover a wide range of dispersed systems, such as solid-liquid (crystallization systems), gas-solid, gas-liquid (aerobic fermentation) and liquid-liquid (food processes) dispersions. Analysis of separation and reactor equipments and dispersed phase reactors, they all involve population balance models [40].

In practical applications, a single bubble size model, as reported by numerous researchers [36, 22], cannot properly describe the interfacial interactions between the phases, and analytical solutions of the PBE are available just for very few and specific cases. Hence, the use of appropriate numerical techniques is unavoidable in order to deal with practical problems. There are several numerical methods satisfying the necessary requirements with respect to robustness and realizability: the quadrature method of moments [34, 33], the direct quadrature method of moments (DQMM) [10], parallel parent and daughter classes (PPDC) [4] and the method of classes [18, 19], which is in the scope of

this study.

In the literature, there are several noticeable breakup and coalescence models. These two competing mechanisms for static conditions finally lead the distribution to a certain dynamic equilibrium. Thus, it is important to have compatible kernels for coalescence and breakage. If one of these kernels is dominant with respect to the other, the achievement of an equilibrium distribution can be unrealistic. Therefore, the breakage and coalescence kernels are usually modeled together. Chen and his co-workers [6] studied the effect of different breakage and coalescence closures and they showed that incompatible kernels produce poor results. Certain experimental and theoretical models for breakage and coalescence kernels are regarded as milestones for the evolution of population balances in the framework of liquid/gas-liquid dispersed phase systems and the evolution of these models is presented in detail by [15].

Most of the present models for coalescence kernels were derived analogously to kinetic theory of gases [9, 45, 39, 30]. In kinetic theory of gases, collisions between molecules are considered while in the process of coalescence, bubble (droplet)–bubble (droplet) and bubble/droplet–eddy collisions count. Thus, various coalescence models show similar trends, that is a monotonous increase in the specific coalescence rate with increase in the bubble/droplet diameter [5]. The coalescence kernel function adopted in this work is the one proposed by Lehr *et al.* [28] which is implemented according to the technique developed by Buwa and Ranade [5].

In the case of breakup, most of the published studies on bubble/droplet breakup are derived from the theories which are outlined by [12] and [16]. All these models have their own advantages and weak points which makes them dramatically different. Nevertheless, they have similar phenomenological interpretations: bubble/droplet breakage occurs due to turbulent eddies colliding with the bubble/droplet surface. If the energy of the incoming eddy is higher than the surface energy, deformation of the surface happens, which may result in breakup of a bubble/droplet into two or more daughter bubbles/droplets. The colliding eddies that are larger than the bubble/droplet result in spatial transportation. Thus, collisions between bubble/droplet and eddies which are smaller than or equal in size to the bubble/droplet, give rise to breakage. The main differences among the available models are due to their predictions of daughter size distributions (DSD). Some of the models assume a uniform or a truncated normal distribution which is centered at the half of the bubble/droplet size. In other words these models are based on the assumption of equal-sized breakage [2, 26, 47]. In contrast, some others presume unequal breakup which means a bubble/droplet breaking into a large and a smaller one [2, 31, 45]. The developed model by [27] is able to combine the features of these significantly different breakage closures. Their model is based on the theoretical findings of [31]. The breakage kernel is derived from the frequency of arriving eddies onto the surface of a bubble and from the probability that collisions lead to breakage. Accordingly, their model predicts an equal-sized breakage for relatively small bubbles/droplets and an unequal-sized breakage for large ones. In fact, their approach appears even intuitively to be reasonable: large

bubbles/droplets firstly collide with large turbulent eddies so that a large and smaller daughter bubble/droplet exists while for small bubbles/droplets equal-sized breakage is easier due to high interfacial forces (large and small are relative to stable bubble size under given conditions). A comprehensive comparison of the noticeable coalescence and breakage models is given by [48]. The comparison shows that the model proposed by [28] is generally superior to other available breakup closures which makes it a suitable candidate for the choice of our breakage kernels.

There are many hydrodynamic variables which affect the efficiency of multiphase reactors. However, one should be able to resolve the flow field in the reactor in order to calculate the necessary breakup and coalescence kernels to solve the population balance equations, that means to solve the transport problems in the internal (size of drops/bubbles) and external (spatial) coordinates. This attempt will involve an inevitable coupling between CFD and PBE which can lead to irrational computational cost and many difficulties in numerics if the problem is not tackled properly.

The dynamics of gas/liquid-liquid dispersed flows has been a topic of research for the last several decades and many different methods were developed. Numerical simulation of flow fields in column reactors, which is a cumbersome problem due to high complexity of the flow field, is possible by adopting the Euler-Euler or Euler-Lagrange approaches. For practical reasons like high numerical efforts and computational costs which are related to tracking and calculating the motion of each bubble individually in the flow field, the former method is restricted to be applied on lean dispersions or when low volume fractions of the dispersed phase are considered, while the latter method requires comparatively small efforts in both numerics and computation. Nevertheless, both of the methods lead to the same results if the problems are handled with adequate computational effort as it has been reported by [44]. Sokolichin and Eigenberger went on with their studies and they elucidated the behavior of flow fields in bubble columns. Numerical simulations which assume the flow to be laminar are not able to produce mesh independent results. The finer the grid, the more vortices are resolved. That is more typical for turbulent flows. Hence, they performed extensive numerical calculations and conducted several experiments after which they concluded that turbulence models are more convenient to describe flow fields in bubble columns [3, 43].

Turbulence models which are applicable to produce results with an acceptable accuracy and reasonable computational cost in general originate from the family of two-equation eddy viscosity models. The most preferred model in this sense is related to the standard or modified k-ε turbulence model which has been implemented in several commercial CFD programs and in-house codes. In most of the present studies which consider implementation of CFD coupled with PBE, it is preferred to work with commercial codes like FLUENT [1, 6, 32, 38] or CFX [5, 7, 28, 27], naming just two of the most important CFD software packages. However, a commercial code is not the only option and open-source software packages such as FeatFlow (see *http://www.featflow.de*) extended with

additional modules (such as turbulence model [20], multiphase model [22], subgrid-scale mixing model [35] or a population balance model in the present case) possess the advantages of higher flexibility and robustness.

The paper is organized as follows. In Section 2 the mathematical model of the population balance equation with the breakage and coalescence kernels is described. In Section 3, the arising standalone implementation of the obtained mathematical model is dealt with. Furthermore, the description of its integration into the CFD flow solver is given in Section 4. The validation of our implementation together with the CFD coupled applications form the content of Section 5, which is followed by our conclusions.

2. Mathematical model

The population balance equation for gas-liquid (liquid-liquid) flows is a transport equation for the number density probability function, f, of bubbles (drops). By definition, f needs to be related to an internal coordinate, what in most of the cases is the volume of bubbles, v. Therefore, the number density, N, and void fraction, α, of bubbles having a volume between v_a and v_b are:

$$N_{ab} = \int_{v_a}^{v_b} f \, dv, \quad \alpha_{ab} = \int_{v_a}^{v_b} f v \, dv. \tag{1}$$

The considered transport phenomena account for convection in the physical space (governed by the flow field $\mathbf{u}_g$), while the bubble breakage and coalescence move the bubbles in the space of the internal coordinate. Thus, the resulting transport equation is the following

$$\frac{\partial f}{\partial t} + \mathbf{u}_g \cdot \nabla f = B^+ + B^- + C^+ + C^-. \tag{2}$$

Clearly, in case of modeling turbulent flows according to (temporal) averaging concepts (2) has to be extended by the arising pseudo diffusion terms in analogy to the approach of the Reynolds stress tensor

$$\nabla \cdot \overline{u' f'} = -\nabla \cdot (\frac{\nu_T}{\sigma_T} \nabla \overline{f}), \tag{3}$$

where σ_T is the so-called turbulent Schmidt number. In (2) the superscripts "+" and "–" stand for sources and sinks and the terms B and C on the right hand side represent the rate of change of the number density probability function, $\left(\frac{\mathrm{d}f}{\mathrm{d}t}\right)$, due to bubble breakup and coalescence, respectively. In this study, both of these processes are modelled in accordance with the two most popular models of Lehr and his colleagues [27, 28] adopting some modifications with respect to an implementation introduced by [5]. According to these studies:

- the breakage of parent bubbles of volume v into bubbles of volume $\tilde{v}$ and bubbles of volume $v - \tilde{v}$ is associated with a rate $r^B(v, \tilde{v}) f(v)$,

- the coalescence of parent bubbles of volume $\tilde{v}$ with bubbles of volume $v-\tilde{v}$ forming bubbles of volume v is associated with a rate $r^C(v-\tilde{v},\tilde{v})f(\tilde{v})f(v-\tilde{v})$,

where r^B and r^C are the so called kernel functions of breakup and coalescence. Substitution of the breakage and coalescence terms into (2) results in the following transport equation

$$\begin{aligned}\frac{\partial f}{\partial t}+\mathbf{u}_g\cdot\nabla f=\int_v^\infty r^B(v,\tilde{v})f(\tilde{v})\,d\tilde{v}-\frac{f(v)}{v}\int_0^v \tilde{v}r^B(\tilde{v},v)\,d\tilde{v}\\ +\frac{1}{2}\int_0^v r^C(\tilde{v},v-\tilde{v})f(\tilde{v})f(v-\tilde{v})\,d\tilde{v}-f(v)\int_0^\infty r^C(\tilde{v},v)f(\tilde{v})\,d\tilde{v},\end{aligned} \tag{4}$$

which still needs to be closed by the specification of the kernel functions r^B and r^C. According to [27] the coalescence kernel function is defined by

$$r^C(v,\tilde{v})=\frac{\pi}{4}(d+\tilde{d})^2\min(u',u_{\text{crit}}), \tag{5}$$

with d and $\tilde{d}$ denoting the diameter of bubbles of v and $\tilde{v}$. The characteristic velocities u' and u_{crit} are computed as follows

$$u'=\sqrt{2}\varepsilon^{1/3}(d\tilde{d})^{1/6}, \tag{6}$$

$$u_{\text{crit}}=\sqrt{\frac{We_{\text{crit}}\sigma}{\rho_l d_{eq}}}\quad\text{with}\quad d_{eq}=2(d^{-1}+\tilde{d}^{-1})^{-1}, \tag{7}$$

where ε is the turbulent dissipation rate, σ is the surface tension of the liquid phase, ρ_l is the density of the liquid phase, and We_{crit} is the critical Weber number being equal to 0.06 for pure liquids [28]. Alternatively, it is also common to assume u'=0.08m/s instead of considering u' to be a function of v and $\tilde{v}$ as it was done in the study of Lehr and his colleagues [28]. However, under certain conditions this assumption seems to lead to unphysical results which are shown and explained in the following section. Additionally, the chosen coalescence kernel (5) shows similar trends (monotonous increase in the specific coalescence rate with increase in bubble diameter) in relation to experimental observations and as most of the other models in the literature [5].

Regarding the breakup kernel there are various different formulations which yield significantly different results. For that reason, it is hard to say that one model can highlight all the features of the given process. A comparison of the most remarkable breakup kernels in the literature is carried out by [48]. In pursuit of the mentioned study it is shown that the model presented by [28] is more comprehensive than any other model in the literature. The model in question [28] is based on the practical formulation of the theoretical findings reported by [31] which therefore forms the fundamental basis of many other relevant breakage models.

Motivated by the wide diversity of available breakage models presented in the literature, we extended our scope by consideration of a second breakage model developed by

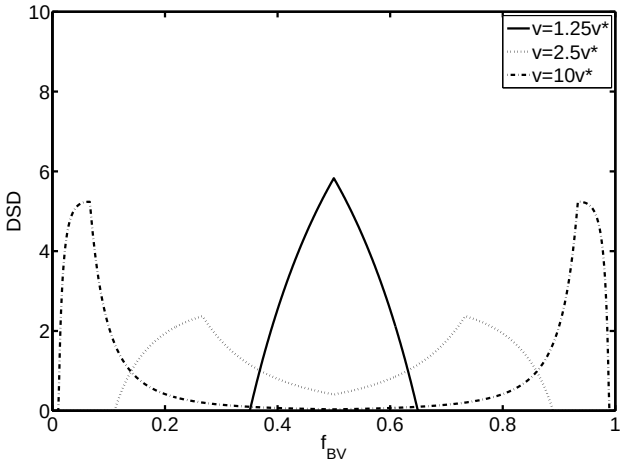

Figure 1: Dimensionless daughter size distribution.

[27]. This model also originates from the pioneering theoretical formulation introduced by [31], that enables us to compare the same theoretical model from the point of view of two different practical interpretations. Additionally, both of the breakage models have the following definition in common

$$r^B(\upsilon, \tilde{\upsilon}) = K^B \Phi(\upsilon, \tilde{\upsilon}), \tag{8}$$

where K^B is the total breakage rate and $\Phi(\upsilon, \tilde{\upsilon})$ is the probability of breaking bubbles of volume υ into bubbles of volume $\tilde{\upsilon}$. The choice of our first breakage closure was influenced by the demonstrated excellent properties of the breakage kernel developed by [27]. As a result of this work, the total breakage rate K^B is defined as

$$K^B = 1.5(1-\alpha_g)\left(\frac{\rho_l}{\sigma}\right)^{2.2}\varepsilon^{1.8}. \tag{9}$$

The aforementioned excellent properties of the adopted breakage kernel are hidden in the definition of the daughter size probability distribution function $\phi(\upsilon, \tilde{\upsilon})$, which naturally provides equal and unequal size distributions for the daughter bubbles (see Fig. 1). Such a behavior of the distribution function is achieved by the following formula

$$\begin{aligned}\phi(\upsilon, \tilde{\upsilon}) = \max\left(\frac{\omega^{1/3}}{\tilde{\omega}^{4/3}}\left(\min\left(\tilde{\omega}^{7/6}, \tilde{\omega}^{-7/9}\right) - \omega^{-7/9}\right), 0\right) \quad \text{for} \quad \frac{\tilde{\omega}}{\omega} \in (0, 0.5\rangle \\ \text{with} \quad \tilde{\omega} = \tilde{\upsilon}\frac{\pi}{6}\frac{\sigma^{1.8}}{\rho_l^{1.8}\varepsilon^{1.2}} \quad \text{and} \quad \omega = \upsilon\frac{\pi}{6}\frac{\sigma^{1.8}}{\rho_l^{1.8}\varepsilon^{1.2}}.\end{aligned} \tag{10}$$

According to the implementation technique developed by [5], the substitution of the dimensionless bubble volume $f_{BV} = \frac{\tilde{\omega}}{\omega} = \frac{\tilde{\upsilon}}{\upsilon}$ into (10) results in

$$\begin{aligned}\phi(\upsilon, \tilde{\upsilon}) = \max\left(\omega^{-1} f_{BV}^{-4/3}\left(\min\left(\left(f_{BV}\omega\right)^{7/6}, \left(f_{BV}\omega\right)^{-7/9}\right) - \omega^{-7/9}\right), 0\right) \\ \text{for} \quad f_{BV} \in (0, 0.5),\end{aligned} \tag{11}$$

and makes it possible to analytically integrate the DSD in arbitrary limits. Being consistent with the assumption that the breakup process results in a pair of daughter bubbles of volume $\tilde{v}$ and $v - \tilde{v}$, this requires symmetry of the function $\phi(v, \tilde{v}) = \phi(v, v - \tilde{v})$ for $f_{BV} \in (0.5, 1)$ (see Fig. 1). Finally, the mean probability of breaking a bubble of volume v into a bubble between $(\tilde{v} - \Delta v)$ and $(\tilde{v} + \Delta v)$ can be obtained as follows

$$\Phi(v, \tilde{v}) = \frac{v}{2\Delta v} \int_{\frac{\tilde{v}-\Delta v}{v}}^{\frac{\tilde{v}+\Delta v}{v}} \phi(v, \tilde{v})\, df_{BV}. \tag{12}$$

The second adopted breakage kernel is the one proposed by [28]. Both, the total breakage rate K^B and the breakage probability $\Phi(v, \tilde{v})$ are defined as a function of the following time and length scales

$$T = \left(\frac{\sigma}{\rho_L}\right)^{0.6} \frac{1}{\varepsilon^{0.4}} \quad \text{and} \quad L = \left(\frac{\sigma}{\rho_L}\right)^{0.4} \frac{1}{\varepsilon^{0.6}}. \tag{13}$$

Introducing the dimensionless bubble diameter $d^* = d/L$ and bubble volume $v^* = v/L^3$ gives rise to:

$$K^B = \frac{d^{*5/3}}{2T} \exp\left(-\frac{\sqrt{2}}{d^{*3}}\right) \tag{14}$$

$$\phi(v, \tilde{v}) = \frac{6}{\left(L\sqrt{\pi}\tilde{d^*}\right)^3} \frac{\exp\left(-2.25\left(\ln\left(2^{2/5}\tilde{d^*}\right)\right)^2\right)}{1 + \operatorname{erf}\left(\ln\left(2^{1/15}d^*\right)^{1.5}\right)} \quad \text{for} \quad \tilde{v}^* \in (0, 0.5\rangle \tag{15}$$

$$\text{and} \qquad \phi(v, \tilde{v}) = \phi(v, v - \tilde{v}) \quad \text{for} \quad \tilde{v}^* \in (0.5, 1) \tag{16}$$

The phenomenological models involve several parameters in their formulations which are strictly depending on the operating conditions and the system. Thus, they are specific to the problem as in the study of [45], whereas in theoretical models formulations do not consist of these empirical parameters; therefore they are supposed to be applicable in a wide range of operating conditions. The explained theoretical breakage closures are chosen due to their applicability in a broad range of operating conditions and similarities in the outline of their formulations, and to show how the peculiarities of these models influence the results of numerical simulations in the validation process.

3. Implementation of PBE

In this study, the discretization of the population balance equation (4) is carried out by the *method of classes* (with piecewise constant approximation functions). The fixed pivot volume of the classes is initialized by specifying the bubble volume of the smallest "resolved" class $v_{\min}$ and the discretization factor q, such that

$$v_i = v_{\min} q^{i-1} \quad \text{with} \quad i = 1, 2, ...n \tag{17}$$

where n is the number of classes. The class width Δv_i is defined by the difference of the upper v_i^U and lower v_i^L limit of the given class i:

$$\Delta v_i = v_i^U - v_i^L \quad \text{with} \quad v_i^U = v_{i+1}^L \quad \text{and} \quad v_{i-1}^U = v_i^L. \tag{18}$$

The limits are fixed and initialized such that in the case of $q = 2$ the pivot volume v_i is centered in the class

$$v_i^U = v_i + \frac{1}{3}(v_{i+1} - v_i), \quad v_i^L = v_i - \frac{2}{3}(v_i - v_{i-1}). \tag{19}$$

The discretized transport equation (4) of the i-th class' number density probability, f_i, results in

$$\begin{aligned} \frac{\partial f_i}{\partial t} + \mathbf{u}_g \cdot \nabla f_i = &\sum_{j=i}^{n} r_{i,j}^B f_j \Delta v_j - \frac{f_i}{v_i} \sum_{j=1}^{i} v_j r_{j,i}^B \Delta v_j \\ &+ \frac{1}{2} \sum_{j=1}^{i} r_{j,k}^C f_j f_k \Delta v_j - f_i \sum_{j=1}^{n} r_{j,i}^C f_j \Delta v_j \qquad \text{for} \quad i = 1, 2, ...n. \end{aligned} \tag{20}$$

The choice of fixed bubble pivot volumes and fixed class widths offers the advantage of expressing the discretized transport equation (20) in terms of class holdups α_i instead of the number probability density, $f_i = \frac{\alpha_i}{v_i \Delta v_i}$ (see (1)). Doing so enforces only mass conservation, however the bubble number density may not be conservative. Regarding the arising inconsistency we subscribe to the argument of [5], who reported that the difference in the predicted values of interfacial area and Sauter mean bubble diameter obtained with only mass conservation and obtained with mass and bubble number conservation was less than 1%. Multiplying equation (20) with $v_i \Delta v_i$ results in conservative source and sink terms, since the overall gas-holdup cannot be changed due to coalescence or breakup procedures[1]. Additionally, any sink (source) term of a given rate associated to a particular breakup or coalescence procedure induces a source (sink) term with the same rate but in a different class. This enables us to assemble only the sink terms while the same contribution is applied to the corresponding source term in the resulting class. Let us for example consider a breakup of bubbles of class i into bubbles of classes j and k. Such a procedure will result in the following right hand sides

$$\begin{array}{lllll} i: & -\left(v_j r_{i,j}^B \Delta v_j \frac{f_i}{v_i}\right) v_i \Delta v_i & -\left(v_k r_{i,k}^B \Delta v_k \frac{f_i}{v_i}\right) v_i \Delta v_i & = & -r_{i,j}^B \alpha_i \frac{v_j \Delta v_j}{v_i} \quad -r_{i,k}^B \alpha_i \frac{v_k \Delta v_k}{v_i} \\ j: & & + \left(v_j r_{i,j}^B f_i \Delta v_i\right) v_j \Delta v_j & = & r_{i,j}^B \alpha_i \frac{v_j \Delta v_j}{v_i} \\ k: & & + \left(v_k r_{i,k}^B f_i \Delta v_i\right) v_k \Delta v_k & = & r_{i,k}^B \alpha_i \frac{v_k \Delta v_k}{v_i} \\ \sum & & & = & 0 \end{array}$$

where $v_k = v_i - v_j$.

However, if we consider the coalescence of bubbles/droplets of the j'th and the k'th class to form bubbles/droplets of the i'th class, to show the conservation of void fraction

is a little bit more tricky. The losses in the k'th and j'th classes due to coalescence with each other are as follows:

$$\begin{aligned} j: &\quad -\left(f_j r^C_{j,k} f_k \Delta v_k\right) v_j \Delta v_j = -r^C_{j,k} \alpha_j f_k \Delta v_k \\ k: &\quad -\left(f_k r^C_{k,j} f_j \Delta v_j\right) v_k \Delta v_k = -r^C_{k,j} \alpha_k f_j \Delta v_j \end{aligned}$$

The gain in the i'th class due to coalescence of the k'th and j'th classes is:

$$i: \quad \tfrac{1}{2}\left(r^C_{j,k} f_j f_k \Delta v_j + r^C_{k,j} f_k f_j \Delta v_k\right) v_i \Delta v_i$$

If we assume that the discretization is equidistant, that means $\Delta v_i = \Delta v_j = \Delta v_k$, and recalling that $v_i = v_j + v_k$ then the following relation is obtained

$$\frac{1}{2}\left(r^C_{j,k} f_j f_k \Delta v_j + r^C_{k,j} f_k f_j \Delta v_k\right)\left(v_j + v_k\right) \Delta v_i = r^C_{j,k} \alpha_j f_k \Delta v_k + r^C_{k,j} \alpha_k f_j \Delta v_j$$

which shows that the sink and source terms of coalescence are also conservative in terms of void fraction. In this study, geometric grids (for the internal coordinate) with varying discretization constants are employed. Therefore, instead of calculating individual sink and source terms due to coalescence, only sink terms for each possible pair of classes are calculated and their sum is added to the resultant bubble class. Accordingly, conservation of mass is enforced from the point of view of coalescence, too.

4. Integration of PBE into CFD

Before proceeding to the description of the developed numerical algorithm, let us recall the problems related to the integration of PBE into a CFD solver. The main problem which has to be clarified at the very first place is based on the identification of the coupling effects between the individual parts of the model (see Fig. 2). Besides the internal coupling of the Navier-Stokes equation (C1 and C2) in case of turbulent flow simulations supported by two-equation eddy viscosity models such as $k-\varepsilon$ models, additional coupling has also to be taken into account (C5). At the same time, as a consequence of multiphase modeling, one has to be aware of even more complex coupling effects due to buoyancy (C7) and enhanced turbulence effects (C8). Furthermore, the turbulence and the multiphase model is coupled by means of the flow field with the Navier-Stokes equation (C5 and C7). Last but not least, internal coupling takes place in all the three subproblems (C1, C3 and C4) resulting in a rather interlocking structure. To cope appropriately with the described strongly coupled system is quite challenging, and may result in unavoidably increased computational cost. Therefore, in this work the coupling effects are relaxed by not taking into account the influence of the turbulence induced by the secondary phase (also known as bubble induced turbulence in gas-liquid systems) and by neglecting the buoyancy forces. Accordingly, the description of a one-way coupled implementation follows which is valid for *a)* pressure driven and *b)* shear induced turbulence dominating systems.

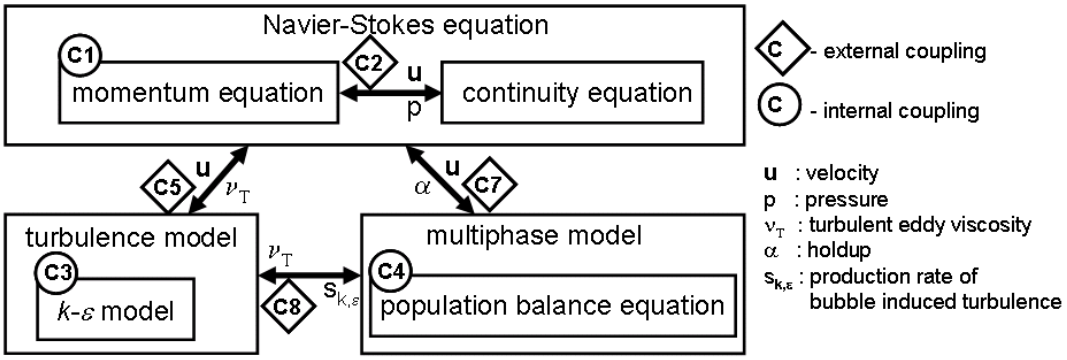

Figure 2: Sketch of the coupling effects inside the complete model.

In this work the motion of fluid flow is governed by the Reynolds Averaged Navier Stokes (RANS) equations of the following form

$$\begin{aligned} &\frac{\partial \mathbf{u}}{\partial t} + \mathbf{u}\cdot\nabla\mathbf{u} = -\nabla p + \nabla\cdot\left((\nu+\nu_T)[\nabla\mathbf{u}+\nabla\mathbf{u}^T]\right), \\ &\nabla\cdot\mathbf{u} = 0, \end{aligned} \tag{21}$$

where ν depends only on the physical properties of the fluid, while ν_T (turbulent eddy viscosity) is supposed to emulate the effects of the unresolved velocity fluctuations $\mathbf{u}'$. According to Chien's Low-Reynolds Number modification of the $k-\varepsilon$ model the eddy viscosity has the following definition

$$\nu_T = C_\mu f_\mu \frac{k^2}{\tilde{\varepsilon}} \quad \text{with} \quad \tilde{\varepsilon} = \varepsilon - 2\nu\frac{k}{y^2}, \tag{22}$$

where k is the turbulent kinetic energy, ε is the dissipation rate and y is the closest distance to the wall[8]. Clearly enough, for computations of k and ε the above PDE system is to be complemented by two additional mutually coupled convection-diffusion-reaction equations [25]. For our purposes, it is worthwhile to introduce a linearization parameter $\gamma = \tau_T^{-1} = \tilde{\varepsilon}/k$, which is related to the turbulent time scale τ_T and which makes it possible to decouple the transport equations as follows [29]

$$\frac{\partial k}{\partial t} + \nabla\cdot\left(k\mathbf{u} - \frac{\nu_T}{\sigma_k}\nabla k\right) + \alpha k = P_k, \tag{23}$$

$$\frac{\partial \tilde{\varepsilon}}{\partial t} + \nabla\cdot\left(\tilde{\varepsilon}\mathbf{u} - \frac{\nu_T}{\sigma_\varepsilon}\nabla\tilde{\varepsilon}\right) + \beta\tilde{\varepsilon} = \gamma C_1 f_1 P_k. \tag{24}$$

The involved coefficients in (23–24) are given by

$$\begin{aligned} &\alpha = \gamma + \frac{2\nu}{y^2}, \quad \beta = C_2 f_2 \gamma + \frac{2\nu}{y^2}\exp(-0.5y^+), \quad P_k = \frac{\nu_T}{2}|\nabla\mathbf{u}+\nabla\mathbf{u}^T|^2, \\ &f_\mu = 1-\exp(-0.0115y^+), \quad f_1 = 1, \quad f_2 = 1-0.22\exp-\left(\frac{k^2}{6\nu\tilde{\varepsilon}}\right)^2. \end{aligned} \tag{25}$$

The discretization in space is performed by a finite element method on unstructured grids. The incompressible Navier-Stokes equations are discretized using the nonconforming $\tilde{Q}_1/Q_0$ element pair, whereas standard Q_1 elements are employed for k and $\tilde{\varepsilon}$. After an implicit time discretization by the Crank-Nicolson, Fractional-step θ scheme or Backward Euler method, the nodal values of $(\mathbf{v}, p)$ and $(k, \tilde{\varepsilon})$ are updated in a segregated fashion within an outer iteration loop.

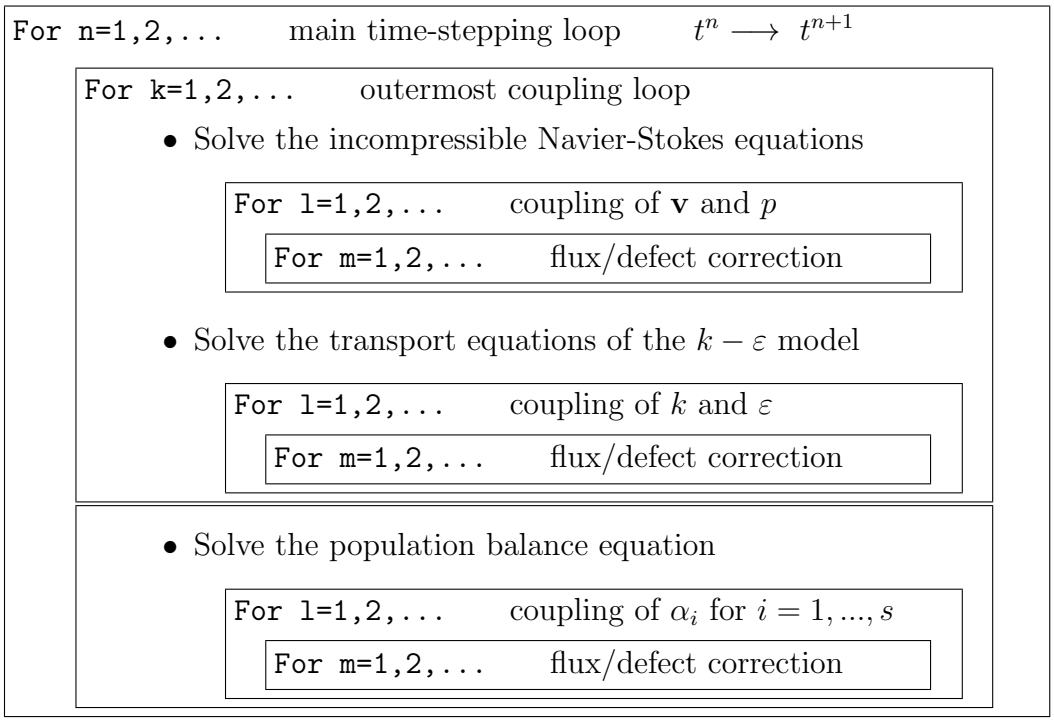

Figure 3: Developed computational algorithm consisting of nested iteration loops.

The iterative solution process is based on the hierarchy of nested loops according to the approach described in [22] and is presented in Fig. 3. At each time step (one $n-$*loop* step), the governing equations are solved repeatedly within the outer k-*loop* which contains the two subordinate l-*loops* responsible for the coupling of variables within the corresponding subproblem. The embedded m-*loops* correspond to iterative flux/defect correction for the involved convection-diffusion operators. In the case of an implicit time discretization, subproblem (23–24) leads to a sequence of algebraic systems of the form [21, 23, 46]

$$\begin{aligned} &A(\mathbf{u}^{(k)}, \gamma^{(l)}, \nu_T^{(k)})\Delta u^{(m+1)} = r^{(m)}, \\ &u^{(m+1)} = u^{(m)} + \omega \Delta u^{(m+1)}, \end{aligned} \tag{26}$$

where $r^{(m)}$ is the defect vector and the superscripts refer to the loop in which the corresponding variable is updated. Flux limiters of TVD type are activated in the vicinity of steep gradients, where nonlinear artificial diffusion is required to suppress nonphysical

undershoots and overshoots. The predicted values $k^{(l+1)}$ and $\tilde{\varepsilon}^{(l+1)}$ are used to recompute the linearization parameter $\gamma^{(l+1)}$ for the next outer iteration (if any). The associated eddy viscosity ν_T is bounded from below by a certain fraction of the laminar viscosity $0 < \nu_{\min} \leq \nu$ and from above by $\nu_{T,\max} = l_{\max}\sqrt{k}$, where $l_{\max}$ is the maximum admissible mixing length (the size of the largest eddies, e.g., the width of the domain). Specifically, we define the limited mixing length l_* as

$$l_* = \begin{cases} C_\mu f_\mu \frac{k^{3/2}}{\tilde{\varepsilon}} & \text{if} \quad C_\mu f_\mu k^{3/2} < \tilde{\varepsilon} l_{\max} \\ l_{\max} & \text{otherwise} \end{cases} \tag{27}$$

and calculate the turbulent eddy viscosity ν_T from the formula

$$\nu_T = \max\{\nu_{\min}, l_*\sqrt{k}\}. \tag{28}$$

The resulting value of ν_T is used to update the linearization parameter

$$\gamma = \tau_T^{-1} = C_\mu f_\mu \frac{k}{\nu_T}. \tag{29}$$

The above representation of ν_T and γ makes it possible to preclude division by zero and to obtain bounded nonnegative coefficients (required by physical reasons and computational stability) without manipulating the actual values of k and ε.

In the following, remarks concerning the treatment of the convection and sink terms in the population balance equation will be given from the point of view of positivity preservation. Since the continuous transport equation (4) is positivity preserving for non-negative initial and boundary conditions the same property needs to be satisfied by its discrete counterpart (20). This can be achieved by an implicit treatment of the sink terms resulting in the following set of equations

$$\begin{aligned} \left(M_L + \left(\theta K - B_i^- - C_i^-\right)\Delta t\right)\alpha_{i,(k+1)}^{(n+1)} &= \left(M_L - (1-\theta)\,K\Delta t\right)\alpha_{i,0}^{(n+1)} + (B_i^+ + C_i^+)\Delta t\alpha_{i,(k)}^{(n+1)} \\ \text{where} \quad \alpha_{i,0}^{(n+1)} &= \alpha_i^n \quad \text{for} \quad i = 1, 2, ...n, \end{aligned} \tag{30}$$

with M_L being the lumped mass matrix, K the discretized convection operator, B and C the discretized breakage and coalescence terms. In case of an implicit time discretization, such as Crank Nicolson or Fractional-step θ time stepping, subproblem (30) leads to the algebraic system of the form [21, 23, 46]

$$\begin{aligned} &A(\mathbf{u}^{(n)}, \nu_T^{(n)}, B_i^{\pm(l)}, C_i^{\pm(l)})\Delta\alpha_i^{(m+1)} = r^{(m)}, \\ &\alpha_i^{(m+1)} = \alpha_i^{(m)} + \omega\Delta\alpha_i^{(m+1)}, \end{aligned} \tag{31}$$

where $r^{(m)}$ is the defect vector and the superscripts refer to the loop in which the corresponding variable is updated (see the algorithm in Fig. 3).

5. Numerical examples

The numerical calculations in scope of this study will be classified into two subsections. The content of the first subsection presents the validation problems, which are supported by experimental and computational results available in the literature. The content of the second subsection deals with a detailed study which couples PBE and CFD in case of a turbulent pipe flow which involves two immiscible fluids.

5.1. Validation problems

In order to validate the implementation of the presented model it is applied to a homogeneous stirred tank reactor in which the turbulent dissipation rate and volume fractions of classes do not exhibit spatial variations. Therefore, transportation of bubbles (droplets) with respect to the spatial coordinate can be neglected and the problem is independent of the flow field. If the values of dissipation rate and gas holdup are fixed for a certain dispersed system, the equilibrium size distribution will be unique regardless of the initial conditions. In pursuit of the described validation technique the case studies described by [11], [42] and [49] will be taken into consideration. Additionally, since the implemented model does not involve any empirical parameters, it should be valid in a wide range of operating conditions. Thus, several other comparisons between our numerical calculations and experimental studies are performed. These experimental studies have been chosen such that the model is tested in broad ranges of turbulent dissipation rates and volume fractions of the secondary phase, which are the most important impact factors. Accordingly, it is possible to demonstrate that the implemented model is applicable for various operating conditions and for different two-phase systems.

The validation process given in this section begins with the problem addressed by [49]. The experimentally measured bubble size distribution corresponding to the mentioned reference study is characterized by the following parameters:

- water-nitrogen system with total gas holdup $\alpha = 0.13$,
- average superficial gas velocity $u_g = 0.04 m s^{-1}$,
- average dissipation rate estimated as $\varepsilon = g u_g = 0.3924 m^2 s^{-3}$.

It should be noted, that Wilkinson's data on bubble size distribution corresponds to the average over the whole reactor, so it does not necessarily reflect the true equilibrium of the bubble breakage and coalescence. Our comparison has been performed on the basis of the bubble number fraction normalized with the group width, $E(d)$, for both adopted breakage models. In order to obtain mesh independent solutions (with respect to the internal coordinate v) the computations were performed for different values of the discretization constant q in a range of 1.05 to 2.0 (see Fig.4). Thus, the number of initialized classes varied between 20 to 100 to cover the required range of bubble sizes. The small differences between the distributions computed on the coarsest ($q = 2.0$) and finest

($q = 1.05$) mesh leads us to the conclusion that qualitatively good results can already be obtained by means of coarse grid computations. As it can be seen from Fig. 5, our computational predictions are in a good agreement with the experimental results of [49] and correlate well with the computational results obtained by [5] (especially in the case of the breakage kernel of [27]) for the same problem and for the same model.

We recall that, in order to obtain the equilibrium between bubble breakup and coalescence for the population balance equation, one might reduce the original system of PDE's to a system of ODE's (neglecting the spatial variation). Then, the steady state solution of such a reduced (0-dimensional) system (stirred tank reactor model) corresponds to the required equilibrium distribution. In Fig. 6, experimentally measured data of this type [11, 42] are presented and compared to our computational predictions. The experiments were conducted with air-water multiphase flow for different volume fractions, $\alpha_1 = 0.2$ and $\alpha_2 = 0.08$, and for the same value of superficial gas velocities $j_{g1} = 0.08ms^{-1}$ and $j_{g2} = 0.02ms^{-1}$ which corresponds to dissipation rates of $0.785m^2s^{-3}$ and $0.196m^2s^{-3}$, respectively. The representative quality of the results was chosen to be the "normalized

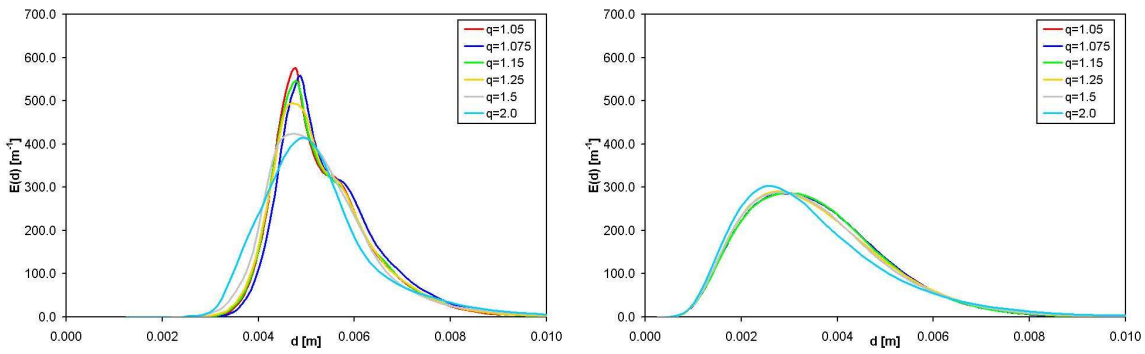

Figure 4: Steady state bubble size distribution for $\alpha = 0.13$ and $\varepsilon = 0.3924m^2s^{-3}$. Right: Breakage kernel [28]. Left: Breakage kernel [27].

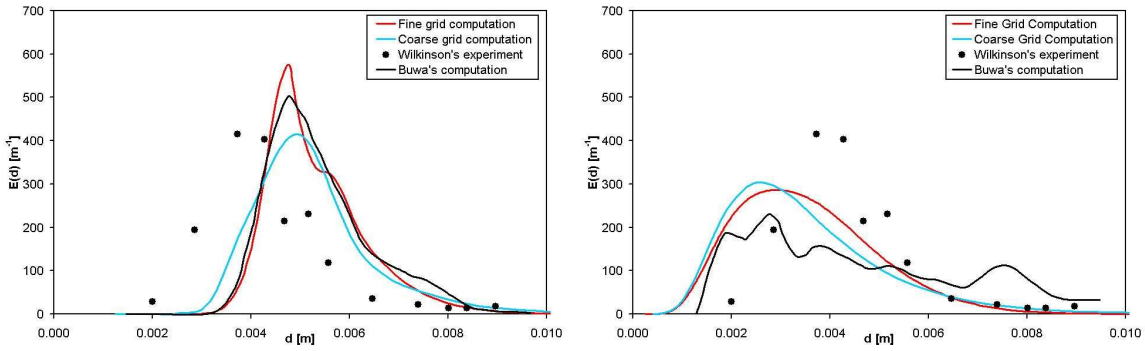

Figure 5: Steady state bubble size distribution for $\alpha = 0.13$ and $\varepsilon = 0.3924m^2s^{-3}$. Comparison of our mesh independent solution with reference data ([49] – experimental, [5] – computational). Right: Breakage kernel [28]. Left: Breakage kernel [27].

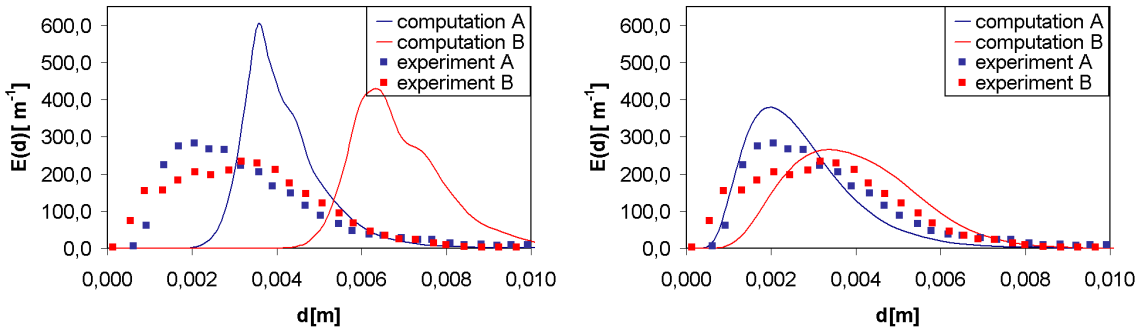

Figure 6: Computed equilibrium distribution for the breakage models versus experimentally measured distribution [11, 42]. Experiment A: $\alpha = 0.2$ and $\varepsilon = 0.785 m^2 s^{-3}$. Experiment B: $\alpha = 0.08$ and $\varepsilon = 0.196 m^2 s^{-3}$. Right: Breakage kernel [28]. Left: Breakage kernel [27].

number of bubbles per fraction width", $E(d)$. We obtained a good agreement between the results of our numerical calculations and the presented experimental results (see Fig. 6). This comparison leads us to conclude that the model by [28] is a more suitable candidate for implementation into our CFD code.

Before progressing to couple PBE with CFD, it is necessary to verify our implementation for high and low turbulent dissipation rates. Thus, two more studies are examined: the first example has been taken from the study by [24] for high dissipation rate values, and the latter one has been taken from the study of Olmos and his colleagues [37] for low values of dissipation rate.

In the first study, the local bubble size distributions (BSDs) had been measured/modelled for dense air–water and CO_2–n-butanol dispersions under hydrodynamic conditions characterized by high turbulent dissipation rates. The experimental [13] and simulation results obtained in the reference study of [24] together with our simulation results corresponding to simulation time of $50s$ are summarized in Tab. 1.

Table 1: Sauter mean diameters (mm)

Case	Hu *et al.*	Laakkonen *et al.*	Our study
air-water	0.447	0.359	0.358
air-1-propanol	0.316	0.207	0.205
air-diethylene glycol	0.598	0.251	0.250

The results are in good agreement with the reference study, in fact they are almost identical. Nevertheless, some remarks are in order. The obtained equilibrium BSDs and the Sauter mean diameters are strongly dependent on the stopping criteria of the iterative scheme. This means that the final Sauter mean diameters may slightly change by varying

the convergence criteria for resulting in different simulation times (stringent criterion – longer simulation and vice versa). Accordingly, the graphs plotted in Fig. 7 show the evolution of the Sauter mean diameter for two different time intervals.

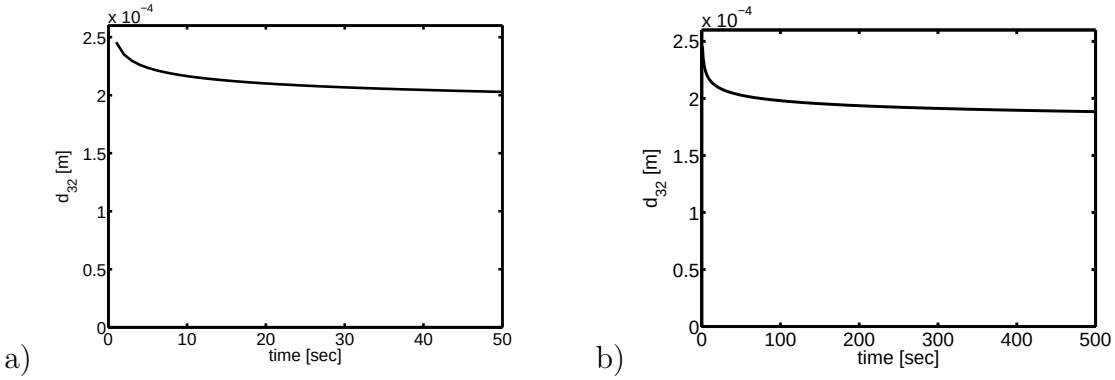

Figure 7: Case: air-1-propanol a) for 50 seconds b) 500 seconds

In Fig. 7(a), the convergence criteria – defined as the maximum relative change of gas holdup of all classes – is of the order of 10^{-7} while in Fig. 7(b), its value has been set to 10^{-8}. It is apparent from the graph corresponding to long time simulation, that the Sauter mean diameter is still changing. Such a behaviour has been already described in the literature by [17], where the steady equilibrium state was not observed even for large time scales. According to the mentioned study and our observations the results tabulated in the original study of Laakkonen would have been more meaningful if the time scales had been specified.

In the second case study, mild and low turbulent dissipation rates are considered. The experimental and numerical results from the study by [37] and the results of our numerical calculations are compared. The comparisons show that our calculations overestimate the

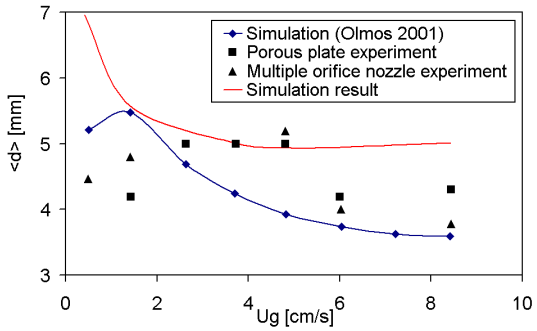

Figure 8: Comparison between experimental and calculated results by [37] and this study.

experimental results of d_{32} with a reasonable error and predict the same behaviour as

observed in experiments. However, for very low turbulent dissipation rates and small gas holdups, predictions of the model become less accurate. Instead of calculating the hydrodynamic variables with a 3D CFD code, as it was done in Olmos's study, the turbulent dissipation rate is assumed to be constant and uniform in the whole domain approximated by the assumption adopted by the study of [27]

$$\varepsilon = j_g g, \tag{32}$$

where j_g is the superficial gas velocity and g is the magnitude of gravitational acceleration. So, rather than performing a detailed calculation for the flow field we only had a rough assumption for the turbulent dissipation rate, nevertheless the obtained results are satisfactory. On the other hand, obtaining hydrodynamic variables with a 3D CFD code will further improve the results.

All these explained studies validate and verify our implementations. However, there are also some important contradictions between our findings and the reference studies of [27] and [28]. In both of these studies, it is claimed that for high superficial gas velocities and gas holdups, a bimodal BSD is observed (that is a BSD with two peaks which are for small and large bubbles). Fig. 9 shows the accumulated gas holdups for one of the cases which involve the bimodal BSD.

In Fig. 9, it is apparent that the largest bubbles are in the largest classes. This result

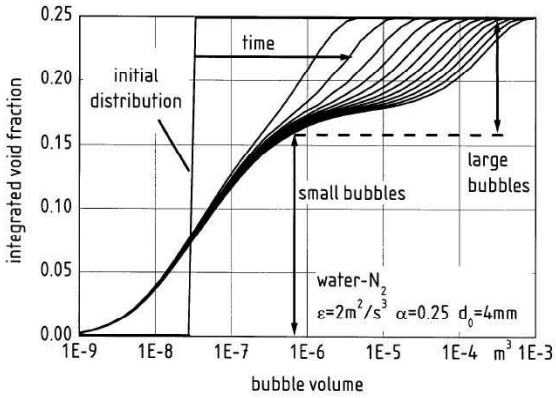

Figure 9: Simulation result of [28] including a bimodal distribution.

may be acceptable but the following question should be also considered: if the size of the largest class in the discretization had been even larger, the evolution of the BSD would have continued and unphysically large bubbles would have occurred. The results of our simulations show that if the model of [28] is considered and u_{crit} equals to $0.08m/s$ then the obtained BSDs have the same features as in the reference study. Accordingly, the BSDs always tend to consist of the largest possible classes, even if the size of the largest classes is unphysically large. Also, the approximation for $u_{\text{crit}} = 0.08m/s$ holds reasonably only for the small bubbles, as it was verified by experimental results in the same study

[28], and generalization of this approximation to large bubbles causes unrealistic results such as having bimodal BSD.

In Fig. 10, it is shown that for the first few seconds, it is possible to have a bimodal

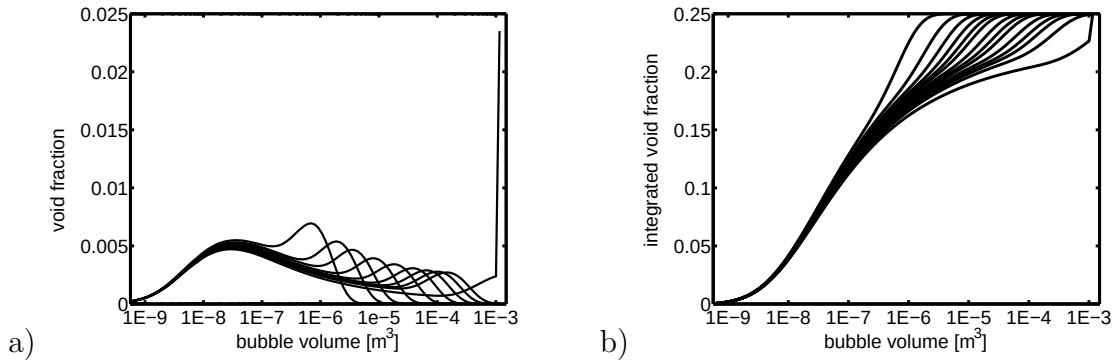

Figure 10: a) bimodal BSD b) bimodal integrated gas holdups

BSD which is **not** in equilibrium, and by time a certain fraction of the gas holdup travels to larger and larger classes to form unreasonably large bubbles. The main idea is if u_{crit} is approximated by $0.08m/s$ then the coalescence dominates the breakage and as a result certain fractions of bubbles coalesce until they reach the largest classes allowing the BSD to reach an equilibrium. However, if u_{crit} is evaluated according to (7), this decreases the rate of coalescence of large bubbles and a true dynamic equilibrium is obtained.

5.2. Coupling with CFD

Up to our knowledge there is no published benchmarked computational result for full three dimensional problems combining CFD and PBE thus first, we restricted our focus to the geometrically most simple 3D problem which involved a turbulent pipe flow and later, an industrial problem, dispersed flow through a Sulzer static mixer SMV$^{\text{TM}}$ was studied to show capabilities of the developed computational tools. Simple pipe problem offers the advantage of validation of the flow field and distribution of turbulent quantities, such as the dissipation rate of the turbulent kinetic energy, ε, which the coalescence and breakage models are most sensitive to. Therefore, in subsection 5.2.1, we aim to reconstruct the underlying turbulent flow field as a prerequisite for a subsequent population balance modeling in the framework of dispersed flows. For this reason, the open-source software package FeatFlow extended with Chien's Low-Reynolds number $k-\varepsilon$ model was utilized to perform the flow simulations, which has already been successfully validated for channel flow problems ($Re_\tau = 395$) [20].

5.2..1 Turbulent pipe flow

The flow considered here is characterized by the Reynolds number, $Re = \frac{dw}{\nu} = 114,000$ (w stands for the bulk velocity), what was influenced by the study of [14] focused on one dimensional dispersed pipe flow modeling. All computational results presented in this

section are obtained by means of an extruded (2D to 3D) unstructured mesh employing 1344 hexahedral elements in each of its layers. The computationally obtained radial distributions of the temporally/spatially developed velocity and turbulent quantities are given in Fig. 11. The turbulent flow field – obtained as described above – was subjected to subsequent three dimensional dispersed flow simulations in a $1m$ long pipe of diameter $3.8cm$. Unfortunately, one has also to say that the computational results following in this section are not compared against any reference data. Hence, our investigation gives just an insight into three dimensional population balance modeling without justified confidence of the obtained results. The considered primary phase was water which contains droplets of another immiscible liquid phase with similar physical properties to water (such as density and viscosity). This assumption together with the fact that the flow is not driven by buoyancy but by the pressure drop enabled us to

- neglect the buoyancy force,
- approximate the dispersed phase velocity with the mixture velocity.

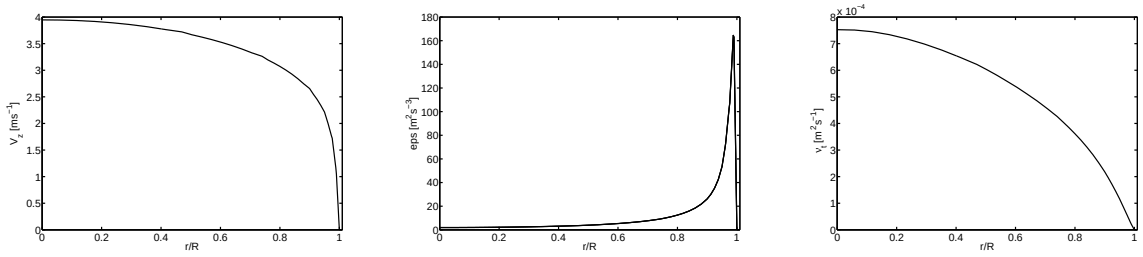

Figure 11: Radial profiles of the axial velocity component (left), turbulent dissipation rate (middle) and turbulent viscosity (right).

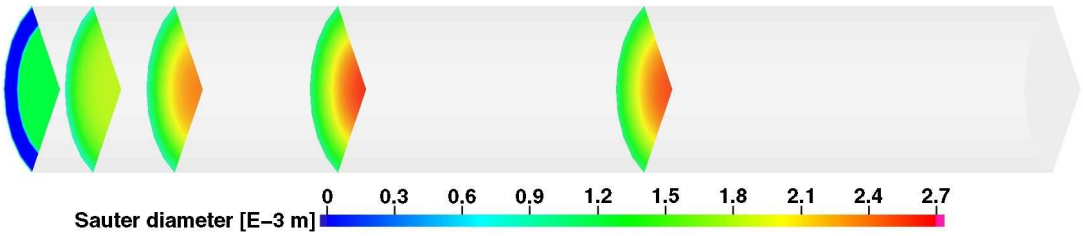

Figure 12: Sauter mean diameter distribution cuts of the dispersed phase at different locations, $x = \{0, 0.06, 0.18, 0.33, 0.6\}$.

The CFD-PBE simulations involved 30 classes initialized by the discretization factor $q = 1.7$, which according to the previous 0D convergence studies turned out to be fine enough to reach mesh independent solutions. The feed stream was modeled as a circular sparger of a diameter of $2.82cm$ containing droplets of a certain size ($d_{in} = 1.19mm$) and of a certain holdup, $\alpha_{in} = 0.55$. Such an inflow holdup condition after reaching developed conditions ensures a flat total holdup distribution of a value $\alpha_{tot} = 0.30$.

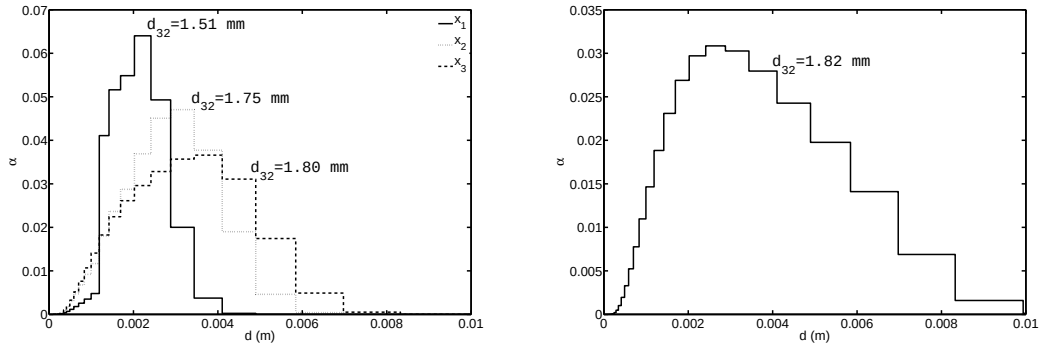

Figure 13: Droplet size distribution at x_1, x_2, x_3 (left) cutplanes and outlet(right), and corresponding sauter mean diameters.

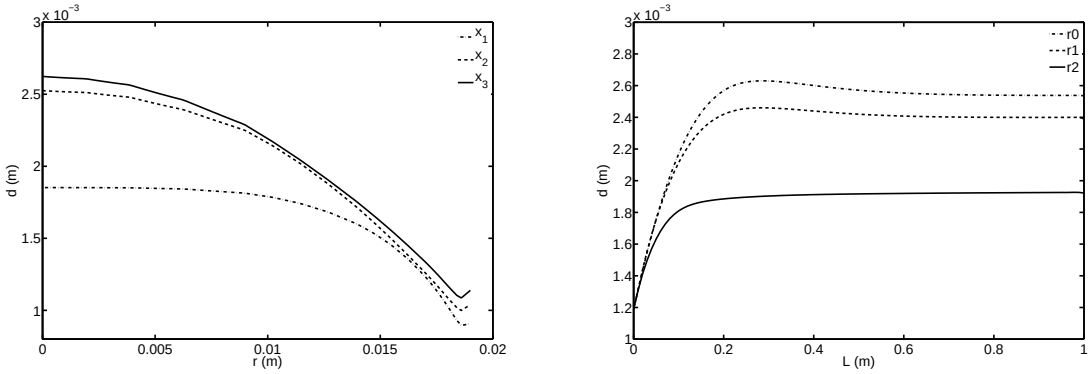

Figure 14: Sauter mean diameter along r at $x = \{0, 0.06, 0.18\}$ (left), along axis at $r_0 = 0$, $r_1 = R/3$ and $r_0 = 2R/3$ (right)

Moreover, according to the developed conditions – as a result of equilibrium between coalescence and breakup – an equilibrium droplet size distribution is reached. This distribution in terms of class holdups vs. droplet size is plotted in Fig. 13. To visualize[2] the evolution of the droplet size distribution in the pipe, Sauter mean diameters of the droplets are plotted (see Fig. 12). Both, the Sauter mean diameter and the droplet size distributions reached the equilibrium at a short distance with respect to length of the pipe. Additionally, as expected, larger droplets are formed in the middle of the pipe (where ε is relatively small), while smaller droplets prevail close to the wall (where ε is relatively high). This fact can be better understood by means of visualization of the representative small/large droplet class-holdup distributions, in Fig. 15. In the mentioned figure the holdup distributions of classes 10, 17 and 23 are depicted[3].

5.2..2 Static Mixer SMV™

Static mixers are tabular internals with optimized geometries to obtain desired dispersions or mixtures while the pressure driven flow is passing through the stationary mixer

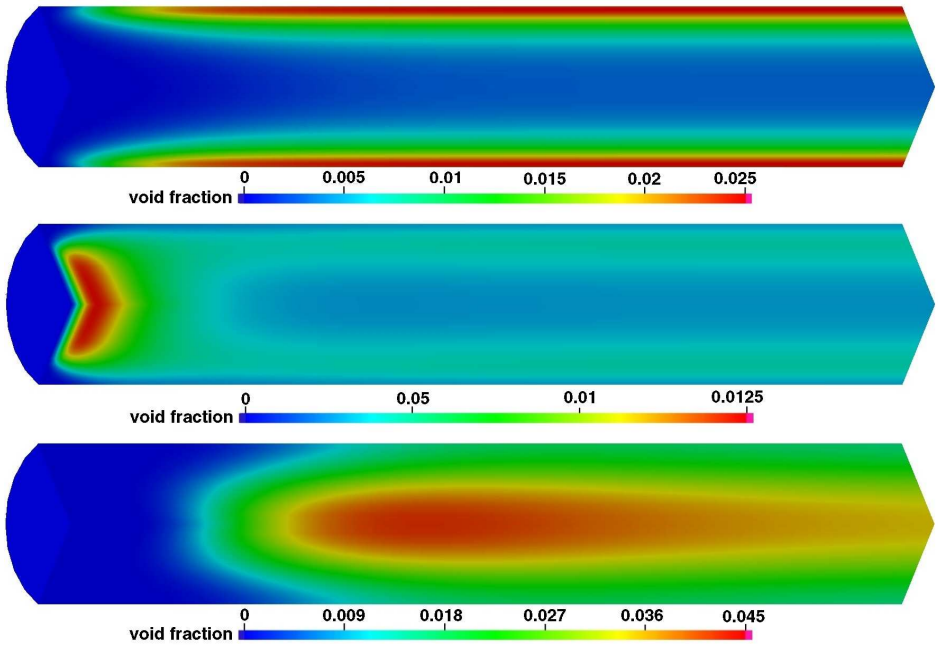

Figure 15: Holdup distributions of certain classes.

elements. Dispersion by static mixers is industrially preferable to dispersion by rotating impellers because it is mechanically simpler and frictional energy dissipation in the packing is more uniform, favoring a more uniform drop size distribution [41]. Narrow size distribution of liquid droplets can be achieved due to the relatively homogeneous flow-field in static mixers so to optimize and control chemical processes. The Sulzer SMV^{TM} mixing elements consist of intersecting corrugated plates and channels, which leads an efficient and rapid mixing action in turbulent flow through the mixer. Therefore, they are ideal for a distributive and homogeneous dispersive mixing and blending action in the turbulent flow regime.

In the literature there are many experimental and computational studies on static mixers in laminar and turbulent flow regimes, a detailed review about static mixers is given by [50]. In our scope, the SMV^{TM} static mixer is studied in order to show the capabilities of the developed computational tools. Therefore, this subsection should be considered as a simple case study rather than a detailed study of a static mixer or verification of implemented models. The verification of developed computational tools which requires intensive experimental work is left as a future study in cooperation with Sulzer Chemtech Ltd..

The static mixer SMV^{TM} is chosen due to its very challenging geometry which makes it a difficult test case for our developed tools. A snapshot of the computational domain which is decomposed into ≈50,000 hexahedral elements, is given in Figure 16.

The inflow condition is a flat velocity profile of value 1 m/s. *Do-nothing* and *no-slip* boundary conditions are prescribed at the outlet and on the walls, respectively. The

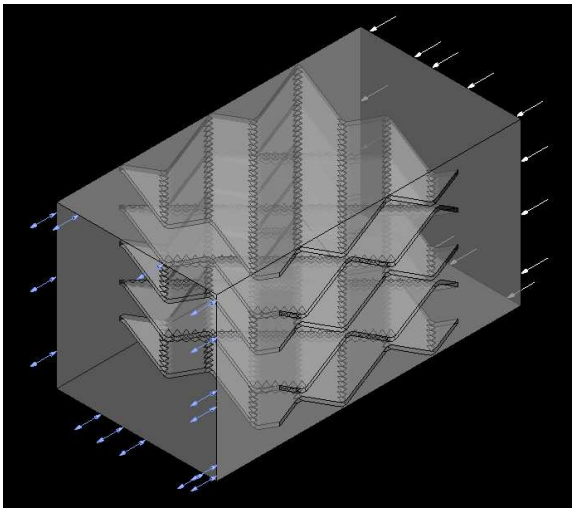

Figure 16: Geometry of SMV^{TM} static mixer.

mixture is oil in water with 0.1 volumetric ratio of oil to mixture. In CFD simulation, the mixture is considered as a single phase whose physical property is weighted average value of phases' physical properties with weight factors being volumetric ratios. Physical properties of the phases are given in Table 2.

Table 2: Physical properties of the phases

Physical properties	Water	Oil
ρ (kgm^{-3})	1000	847
ν (kgm^{-1}s^{-1})	1x10^{-3}	32x10^{-3}
σ (Nm^{-1})	72x10^{-3}	21x10^{-3}
d_{32} (m)	–	1x10^{-3}

Due to high computational costs, a stationary one-way coupled CFD-PBE approach is adopted for calculations. First, the turbulent flow field is simulated and a quasi-stationary solution is obtained, Figure 17.
Then, PBEs are calculated on this stationary flow field with 45 classes where discretization constant q is 1.4 and the smallest class has the size of 0.5 mm. Figure 18.

Time and space averaged experimental data are provided at the cross section right after the mixer element by Sulzer Chemtech Ltd.. Measured droplets are assigned to corresponding classes of the numerical calculation. Since the number of classes in the numerical calculation is too large to obtain representative number of droplets per each class, both numerical results and experimental results are mapped to a coarser internal coordinate which covers the same interval with 15 classes; both results are given in Figure 19.

We can conclude that the experimental result could be predicted within the same order of magnitude by the developed computational tools. Result of the numerical simulation can be improved with more detailed CFD analysis and some minor modifications to the

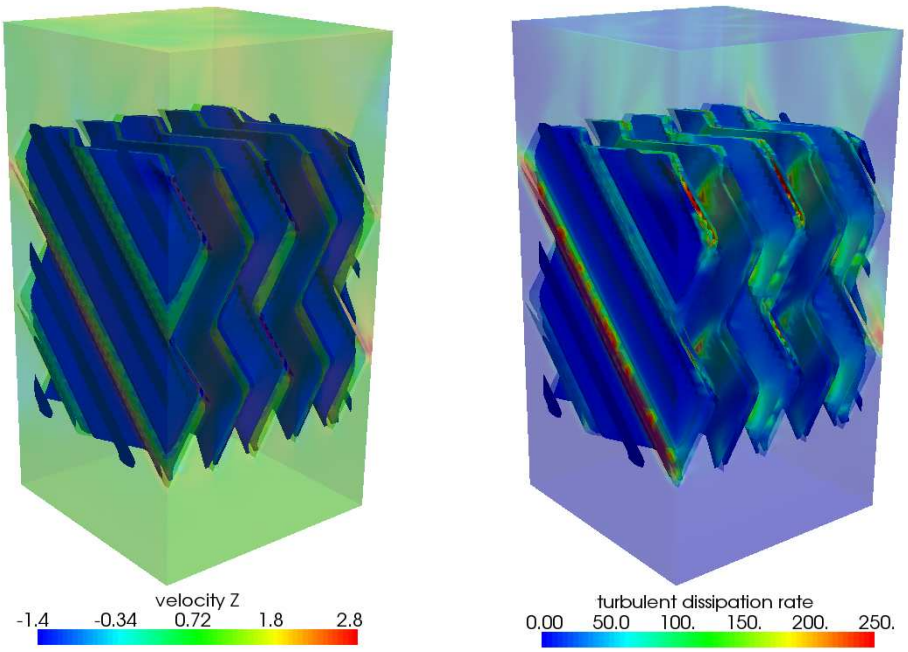

Figure 17: Velocity in z direction (right) and turbulent dissipation rate (left).

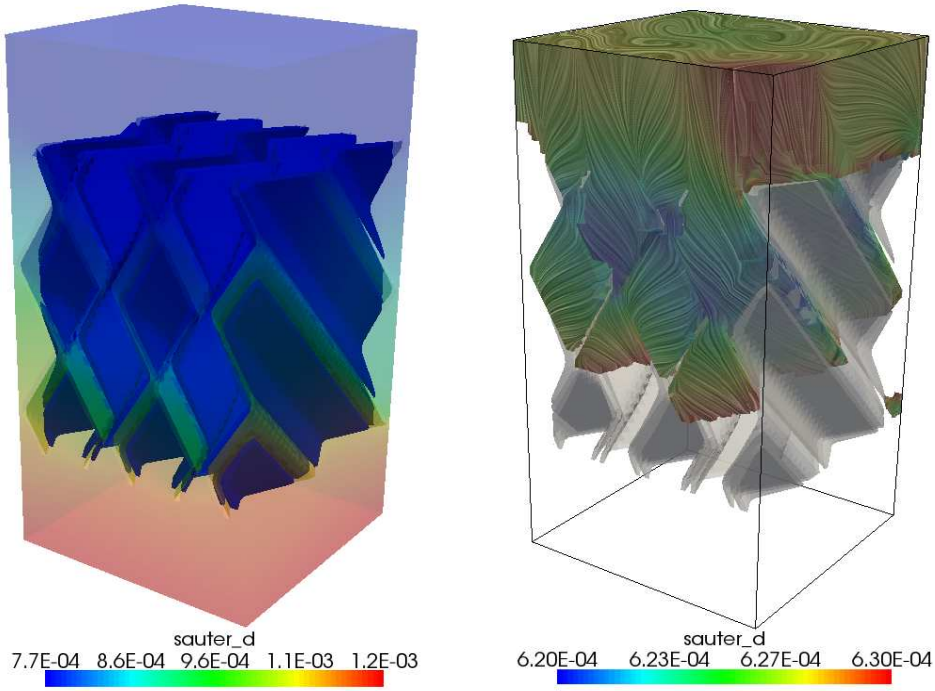

Figure 18: d_{32} values of the droplet ensembles (left). Droplet ensembles with $d_{32} = [0.62, 0.63]$ mm (right).

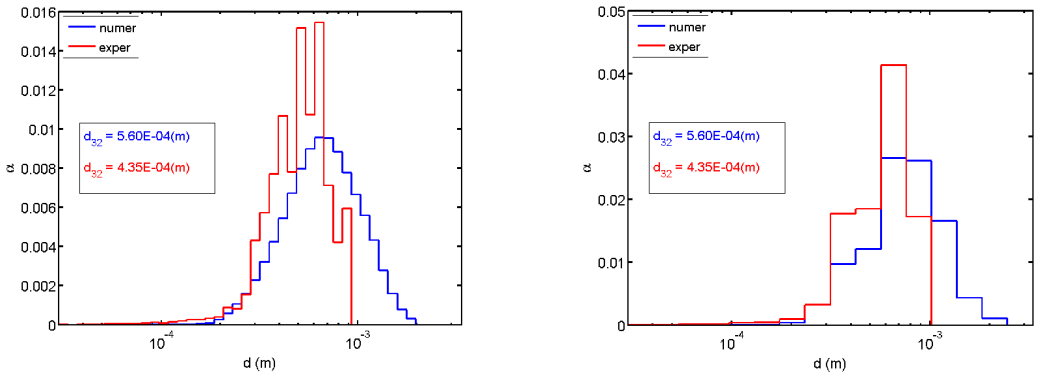

Figure 19: Experimental and numerical results for holdup distribution of dispersed phase with 45 (left) and 15 (right) classes.

implemented population balance model like, an additional term to suppress the coalescence. However, these issues are subscribed to our future studies. With this case study, it is shown that implemented models are valid and the developed computational tools can be employed to elaborately study liquid/liquid dispersed phase systems in complex geometries as, static mixers.

6. Conclusions

In this work, the population balance equation describing two phase dispersed flows was integrated into our in-house CFD software package FeatFlow enriched with the low Reynolds k–ε turbulence model. The models of two breakage and one coalescence kernels were implemented and validated for simple 0D examples. The obtained results are in good agreement with the computational and experimental results previously reported (Fig. 4, Fig. 5). Finally, 3D computational studies were performed for turbulent flows in a simple pipe and through the Sulzer SMV$^{\text{TM}}$ static mixer. The extensive computational costs for the calculation of the hydrodynamic variables coupled with PBE may require alternative approaches in future. First of all, the use of PPDC or DQMM may reduce the computational cost for solving the transport equation of PBE in the internal coordinate, while parallelization of the implemented model in terms of domain decomposition will enable us to obtain results in considerably shorter time. Moreover, instead of solving all the transport equations on the same mesh, a coarser one may be used to obtain mesh independent solution for the PBE. For this purpose, one can take advantage of multigrid techniques implemented in FeatFlow. Additional to our concerns of computational performance, we consider extending our implementation to include two-fluid and/or multifluid approaches and take into account buoyant forces in order to have a more comprehensive model. So that, turbulent dispersed flows can be elaborately studied in complex geometries.

7. Acknowledgements

This work is partially supported by the German Research Association (DFG) through the grant TU 102/2-3.

The authors thank to Sebastian Hirschberg from Sulzer Chemtech Ltd. for providing experimental data.

References

[1] Alexiadis A., Gardin P. and Domgin J. F., *Probabilistic approach for break-up and coalescence in bubbly-flow and coupling with CFD codes*, Applied Mathematical Modeling, **31**, 2007, pp.2051- 2061.

[2] Martínez-Baźan C., Montañés J. L., and Lasheras J. C., *On the breakup of an air bubble injected into a fully developed turbulent flow. Part 2. Size PDF of the resulting daughter bubbles*, Journal of Fluid Mechanics, **401**, 1999, pp.183-207.

[3] Borchers O., Busch C., Sokolichin A. and Eigenberger G., *Applicability of the standard k-ε turbulence model to the dynamic simulation of bubble columns. Part II: Comparison of detailed experiments and flow simulations*, Chemical Engineering Science, **54**, 1999, pp.5927-5935.

[4] Bove S., *Computational fluid dynamics of gas-liquid flows including bubble population balances*, PhD Thesis, Aalborg University, Denmark, 2005.

[5] Buwa V. V. and Ranade V. V., *Dynamics of gas-liquid flow in a rectangular bubble column: experiments and single/multi-group CFD simulations*, Chemical Engineering Science, **57**, 2002, pp.4715-4736.

[6] Chen P., Sanyal J., Dudukovic̀ M. P., *Numerical simulation of bubble columns flows: effect of different breakup and coalescence closures*, Chemical Engineering Science, **60**, 2005, pp.1085-1101.

[7] Cheunga S. C. P., Yeoh G. H. and Tu J. Y., *On the modelling of population balance in isothermal vertical bubbly flows. Average bubble number density approach*, Chemical Engineering and Processing, **46**, 2007, pp.742-756.

[8] Chien K. Y., *Predictions of channel and boundary-layer flows with a low-Reynolds-Number Turbulence Model*, *AIAA J.* **20**, 1982, pp.33-38.

[9] Coulaloglou C. A. and Tavlarides L. L., *Drop size distributions and coalescence frequencies of liquid-liquid dispersions in flow vessels*, AIChE Journal, **22**-2, 1976, pp.289-297.

[10] Fan R., Marchisio D. L. and Fox R. O., *Application of the direct quadrature method of moments to polydisperse gas-solid fluidized beds*, Journal of Aerosol Science, **139**, 2004, pp.7-20.

[11] Grienberger J. and Hofmann H., *Investigation and modelling of bubble columns,* Chemical Engineering Science, **47**, 1992, pp.2215-2220.

[12] Hinze J. O., *Fundamentals of the hydrodynamic mechanism of splitting in dispersion processes*, AIChE Journal, **1**, 1955, pp.289-295.

[13] Hu B., Pacek A.W., Stitt E.H. and Nienow A.W., *Bubble sizes in agitated air alcohol systems with and without particles: turbulent and transitional flow*, Chemical Engineering Science, **60**, 2005, pp.6371-6377.

[14] Hu B., Matar O. K., Hewitt G. F.and Angeli P., *Population balance modelling of phase inversion in liquid-liquid pipeline flows*, Chemical Engineering Science, **61**-15, 2006, 4994-4997.

[15] Jakobsen H. A., Lindborg H., and Dorao C. A., *Modeling of bubble column reactors: progress and limitations*, Industrial Engineering and Chemical Research, **44**, 2005, pp.5107-5151.

[16] Kolmogorov A. N., *On the breakage of drops in a turbulent flow*, Dokl. Akad. Navk. SSSR, **66**, 1949, pp.825-828.

[17] Kostoglou M. and Karabelas A.J., *Toward a unified framework for the derivation of breakage functions based on the statistical theory of turbulence*, Chemical Engineering Science, **60**, 2005, pp.6584-6595.

[18] Kumar S. and Ramkrishna D., *On the solution of population balance equations by discretization - I. A fixed pivot technique*, Chemical Engineering Science, **51**-8, 1996, pp.1311-1332.

[19] Kumar S. and Ramkrishna D., *On the solution of population balance equations by discretization - II. A moving pivot technique*, Chemical Engineering Science, **51**-8, 1996, pp.1333-1342.

[20] Kuzmin D., Mierka O. and Turek S., *On the implementation of the k-epsilon turbulence model in incompressible flow solvers based on a finite element discretization*, International Journal of Computing Science and Mathematics, **1**-2/3/4, 2007, pp.193-206.

[21] Kuzmin D. and Möller M., *Algebraic flux correction I. Scalar conservation laws*, In: D. Kuzmin, R. Löhner and S. Turek (eds.), *Flux-Corrected Transport: Principles, Algorithms, and Applications*, Springer, Germany, 2005, pp.155-206.

[22] Kuzmin D. and Turek S., *Numerical simulation of turbulent bubbly flows,* In: Proceedings of the Third International Symposium on Two-Phase Flow Modeling and Experimentation, Pisa, Italy, 2004.

[23] Kuzmin D. and Turek S., *Multidimensional FEM-TVD paradigm for convection-dominated flows, Technical report* **253**, TU Dortmund. In: *Proceedings of the IV European Congress on Computational Methods in Applied Sciences and Engineering (ECCOMAS)*, 2004, Volume II, ISBN 951-39-1869-6.

[24] Laakkonen M., Moilanen P., Alopaeus V. and Aittamaa J. *Modelling local bubble size distributions in agitated vessel*, Chemical Engineering Science, **62**, 2007, pp.721-740.

[25] Launder B. and Spalding D., *The numerical computation of turbulent flows,* Computer Methods in Applied Mechanics and Engineering **3**, 1974, pp.269-289.

[26] Lee C. H., Erickson L. E., and Glasgow L. A., *Dynamics of bubble size distribution in turbulent gas liquid dispersions*, Chemical Engineering Communications, **61**, 1987, pp.181-195.

[27] F. Lehr and D. Mewes, *A transport equation for interfacial area density applied to bubble columns*, Chemical Engineering Science, **56**, 2001, pp.1159-1166.

[28] Lehr F., Millies M. and Mewes D., *Bubble size distribution and flow fields in bubble columns*, AIChE Journal, **48**-11, 2002, pp.2426-2442.

[29] Lew A. J., Buscaglia G. C. and Carrica P. M., *A note on the numerical treatment of the k-epsilon turbulence model,* Int. J. of Comp. Fluid Dyn., **14**, 2001, pp.201-209.

[30] H. Luo, *Coalescence, break-up and liquid circulation in bubble column reactors*, PhD. Thesis, The Norwegian Institute of Technology, Norway, 1993.

[31] Luo H. and Svendsen H. F., *Theoretical model for drop and bubble breakup in turbulent dispersions*, AIChE Journal, **42**, 1996, pp.1225-1233.

[32] Marchisio D. L., Vigil R. D. and Fox R. O., *Implementation of the quadrature method of moments in CFD codes for aggregation breakage problems*, Chemical Engineering Science, **58**, 2003, pp.3337-3351.

[33] McGraw R. and Wright D. L., *Chemically resolved aerosol dynamics for internal mixtures by the quadrature method of moments*, Journal of Aerosol Science, **34**, 2003, pp.189-209.

[34] McGraw R., *Description of aerosol dynamics by the quadrature method of moments*, Aerosol Science and Technology, **27**, 1997, pp.255-265.

[35] Mierka O., *CFD modelling of chemical reactions in turbulent liquid flows*, Ph.D. Thesis, Slovak Technical University, Slovakia, 2005.

[36] Millies M. and Mewes D., *Interfacial area density in bubbly flow*, Chemical Engineering and Processing, **38**, 1999, pp.307-319.

[37] Olmos E., Gentric C., Vial Ch., Wild G. and Midoux N., *Numerical simulation of multiphase flow in bubble column reactors. Influence of bubble coalescence and break-up*, Chemical Engineering Science, **56**, 2001, pp.6359-6365.

[38] Öncül A. A., Niemannb B., Sundmacher K. and Thévenin D., *CFD modelling of BaSO4 precipitation inside microemulsion droplets in a semi-batch reactor*, Chemical Engineering Journal, **138**, 2008, pp.498-509.

[39] Prince M. J. and Blanch H. W., *Bubble coalescence and break-up in air-sparged bubble columns*, AIChE Journal, **36**, 1990, pp.1485-1499.

[40] Ramkrishna D., *Population Balances: Theory and Applications to Particulate Systems Engineering*, Academic Press, USA, 2000.

[41] Rama Rao N.V., BairdM.H.I., Hrymak A.N. and Wood P.E.; *Dispersion of high-viscosity liquidliquid systems by flow through SMX static mixer elements* Chemical Engineering Science, **62**, 2007, pp. 6885-6896.

[42] Schrag H. J., *Blasengrössen-Häufigkeitsverteilungen bei der Begasung von Gemischen organisch-chemischer Flüssigkeiten mit Stickstoff in Blasensäulen-Reaktoren*, PhD Thesis, University Aachen, Germany, 1976.

[43] Sokolichin A. and Eigenberger G., *Applicability of the standard k-ε turbulence model to the dynamic simulation of bubble columns. Part I: Detailed numerical simulations*, Chemical Engineering Science, **54**, 1999, pp.2273-2284.

[44] A. Sokolichin, Eigenberger G., Lapin A. and Lbert A., *Dynamical numerical simulation of gas-liquid two-phase flows Euler/Euler versus Euler/Lagrange*, Chemical Engineering Science, **52**-5, 1997, pp.611-626.

[45] Tsouris C. and Tavlarides L. L., *Breakage and coalescence models for drops in turbulent dispersions*, AIChE Journal, **40**, 1994, pp.395-406.

[46] Turek S. and Kuzmin D., *Algebraic Flux Correction III. Incompressible Flow Problems*, In: Kuzmin D., Löhner R. and Turek S. (eds.) *Flux-Corrected Transport: Principles, Algorithms, and Applications*, Springer, Germany, 2005, pp.251-296.

[47] Valentas K. J., Bilous O., and Amundson N.R., *Analysis of breakage in dispersed phase systems*, Industrial Engineering Chemistry Fundamentals, **5**, 1966, pp.271-279.

[48] Wang T., Wang J. and Jin Y., *A novel theoretical breakup kernel function for bubbles/droplets in a turbulent flow*, Chemical Engineering Science, **58**, 2003, pp.4629-4637.

[49] Wilkinson P. M., *Physical aspects and scale-up of high pressure bubble columns*, PhD Thesis, University Groningen, The Netherlands, 1991.

[50] Thakur R. K., Vial Ch., Nigam K. D. P., NAUMAN E. B. and Djelveh G. *Static Mixers in the process industries–A Review* Trans IChemE, **81**, 2003, pp.787-826.

Nomenclature

A	global operator
B	source/sink terms due to breakup
C	source/sink terms due to coalescence
C_1, C_2	model constants
d	diameter
f	number density probability function
f_{BV}	bubble/droplet volume fraction
f_1, f_2, f_μ	damping functions
$\mathbf{g}$	gravitational acceleration
k	turbulent kinetic energy
K	rate (with superscript)
K	discrete convective operator
l_*	limited mixing length
L	length scale
M_L	lumped mass matrix
n	number of classes
N	number density
q	discretization factor
r	kernel
T	time scale
$\mathbf{u}$	velocity
u'	characteristic velocity
$\mathbf{u}'$	fluctuating velocities
u_{crit}	critical velocity
We_{crit}	critical Weber number
y	closest distance to wall

Greek letters

α	void fraction
γ	linearization parameter
Δv	class width
ε	turbulent dissipation rate
θ	Fractional-step parameter
ρ	density
ν_T	eddy viscosity
σ_T	turbulent Schmidt number
τ_T	turbulent time scale
v	volume
σ	surface tension

ϕ	probability distribution function
Φ	breakage probability
ω	dimensionless bubble/droplet volume

Subscripts

a, b	lower, upper limits
ab	interval between a and b
g	gas
i, j	class indices
l	liquid

Superscripts

B, C	breakage, coalescence
$\sim$	daughter bubble/droplet
$+, -$	source, sink
l, u	lower,upper limit of classes
$+, -$	source, sink
$*$	dimensionless variables